Reverse Time Migration of Marmousi Model

Nicholas Dorogy, GPGN 536

INTRODUCTION

Seismic reverse time migration (RTM) is a technique used to estimate the Earth's subsurface structure using wave reflection data. By solving the wave equation through a given medium, we are able to simulate the propagation of incident and scattered waves. Then, by implementing an imaging condition that relates these incident and scattered waves, the reconstruction of subsurface structures can be estimated regardless of the body's velocity profile and accompanying reflection boundaries. For this reason, RTM is a powerful high fidelity methodology for analyzing the subsurface.

METHODOLOGY

When implementing the reverse time migration process, a series of source and receiver pairings can be used to simulate wave emitters and recorders to reconstruct the reflection boundaries of an unknown medium. The theoretical process is relatively straightforward. A signal fired from a source will propagate through the field and the signals (or waveforms) "felt" at each receiver location are recorded. The signals recorded at each receiver are then reversed in time and propagated into the medium from the corresponding receiver locations. That is, the last signal arriving at the receiver location is the first to be re-injected into the model. Figure 1 displays a example snapshot of the receiver-recorded waveforms being re-injected into the medium.

Once re-injection has been computed for all time steps, the resulting re-injected waveforms must be reversed in time again (or, alternatively, the incident wave data must be time-reversed). This is because the original forward propagation and the re-injected receiver waveforms will be multiplied at all time steps. This effect is equivalent to cross correlating the forward and reverse waves and thus requires the re-injected data to begin from t=0 to match the time evolution of the forward data. The result is a multiplication of two signals that are only both non-zero at the location at which they were reflected. In other words, the forward waveform is multiplied by its reflection data for all time steps and the result provides a non-zero value only at the location where the two waves intersect, the reflection point. The summation of this cross correlation process for all of the previously simulated time steps provides a detailed image of all reflection boundaries encountered in the medium. Moreover, repeating this process for sources at a variety of locations increases the model's spatial fidelity by introducing more signals to be interact with boundaries and by better sampling boundaries at steep angles with respect to the original source point. Better sampling of structures at greater distances from the source location simply requires the model be given sufficient time to reach and interact with these boundaries.

Equations

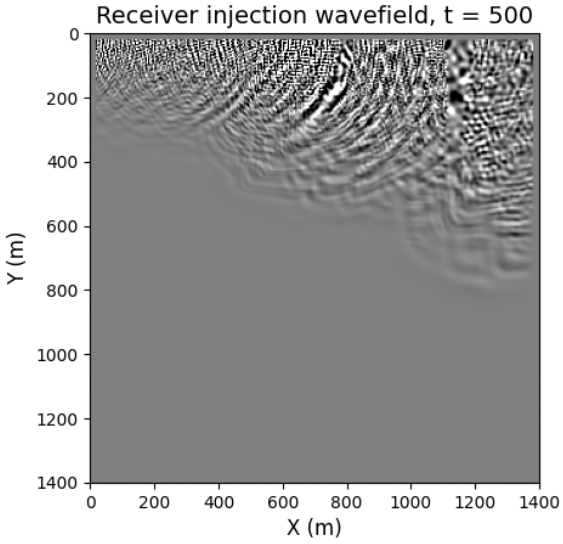

Figure 1: The wavefield produced after 500 model seconds as a result of the re-injection of the signals recorded by each receiver at the receivers' location using a single original source located at [x=560m,y=28m].

To propagate a wave in a two dimensional acoustic medium, a hyperbolic partial differential equation must be solved. To complete this process computationally, a discretized version of the wave equation must be introduced. In this model, I utilize an eighth-order heterogeneous wave equation. This process is used because higher order estimations increase the accuracy of the solution by more faithfully accounting for the second order derivative approximation in the wave equation. Alternatively, smaller spatial steps can increase model accuracy, but subsequently increase computation time to ($\mathcal{O}(N^3)$). Higher order approximation methods circumvent these significant computational time increases. The eighth-order homogeneous approximation is given by,

$$\phi_{i,j}^{n+1} = 2\phi_{i,j}^{n} - \phi_{i,j}^{n-1} + C_x^2 \sum_{k=-4}^{4} c_k \phi_{i+k,j}^{n} + C_y^2 \sum_{k=-4}^{4} c_k \phi_{i,j+k}^{n} + \Delta t^2 F_{i,j} \tag{1}$$

and uses the four surrounding points to the left and right of center, as well as the four surrounding points above and below the center to develop an approximation for the value at the center point for the following time step. A boundary condition consisting of 0's and occupying the four elements closest to the boundaries is implemented. These points handle the end case so that the model does not search for non existent values

outside of the model space. The zero values create reflecting boundaries, but non-zero boundary values could also be implemented to simulate absorption into the surrounding material.

Furthermore, to implement the heterogeneity of the velocity wavefield, a spatially varying velocity function is introduced into the wave equation. The resulting value for each discretized point in the medium is then given by,

$$\phi_{i,j}^{n+1} = 2\phi_{i,j}^{n} - \phi_{i,j}^{n-1} + \left(\frac{v_{i,j}\Delta t}{\Delta x}\right)^2 \sum_{k=-4}^{4} c_k \phi_{i+k,j}^{n} + \left(\frac{v_{i,j}\Delta t}{\Delta y}\right)^2 \sum_{k=-4}^{4} c_k \phi_{i,j+k}^{n} + \Delta t^2 F_{i,j} \quad (2)$$

This equation successfully estimates the wave propagation in the medium for any input source (that is, for either incident or reflected waves) and is the solution to the discretized eighth-order **heterogeneous** wave equation.

Aside from the model's wavefield evolution conditions provided by the eighth order wave approximation, a wave signal must also be introduced to transmit into the medium. The forward model employs a Ricker wavelet to propagate through the medium and is given by,

$$f(x) = (1 - \frac{(t - t_0))}{\sigma})^2 e^{\frac{(t-t_0)^2}{2\sigma^2}} \quad (3)$$

It is important to note that the reverse time migration utilizes recorded wave signal traces and thus therefore does not need the Ricker wavelet signal during the re-injection step. In addition, the RTM process outlined in the previous section can mathematically be described by,

$$I = \sum_{i}^{N} \sum_{t}^{M} SF(x,y,t) SR(x,y,t) \quad (4)$$

where $SF(x,y,t)$ describes the forward modeled two dimensional wavefield at time t and $SR(x,y,t)$ provides the time inverted two dimensional reflection wavefield model at time t.

Finally, to ensure model stability and limit numerical dispersion, the Courant number was carefully handled to be no greater than 0.5. The Courant number is given by,

$$C = \frac{c\Delta t}{\Delta x} \quad (5)$$

and mathematically encodes that the time step, Δt, must be smaller than the time taken for the wave to travel the distance of the spatial step, Δx, in order to to create stable solution.

METHODOLOGY

To test the reverse time migration process, I utilize the Marmousi model and its corresponding velocity profile as shown in Figure 2. Receivers were simulated at every point along the x-axis (every column) at a depth of 28 meters and sources were simulated at a depth of 28 meters and at evenly spaced, repeating intervals of 28 meters along the x-axis. The yellow stars in Figure 2 represent source locations in the Marmousi model, while the green triangles represent receiver locations. Note that the green stars appear to be a line because they are so densely packed together at every point along the x-axis.

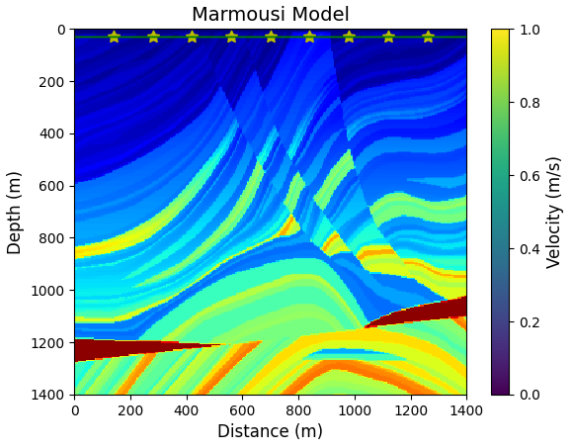

Figure 2: The Marmousi subsurface velocity model. Yellow stars indicate source locations, while green triangles indicate receiver positions.

Several alternate models with variable source location testing were also tested for comparison. For *all* implementations of this model, the Ricker wavelet time shift, t_0, was 0.05 and the time duration of the wave, σ, was 0.001. Furthermore, the model was implemented with a time discretization of 4.2ms, spatial discretization along the x-axis 0f 4.667, and spatial discretization along the y-axis of 4.697. As a result, the Courant number was 0.5.

RESULTS

Figure 3 displays the results of the RTM process performed on the standard configuration after it is run for 3,000 model seconds.

When comparing this result against the original Marmousi model, it is clear that the same predominant features can be seen in both images. Figure 4 is an overlay that highlights some of the major structures present in both images.

A second implementation of the standard model that has been simulated for 500 model seconds is displayed in Figure 5 below. Figure 6 displays the accompanying RTM and Marmousi overlay.

From these image it is clear that neither RTM solution is able

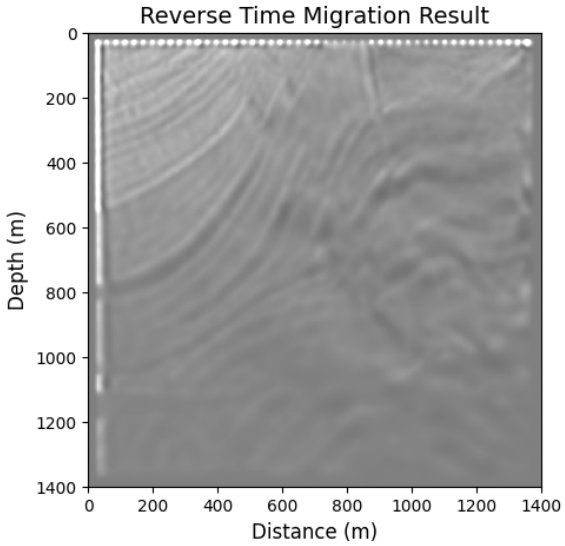

Figure 3: RTM result after running the simulation for 3,000 model seconds with 50 evenly distributed sources at 28m intervals.

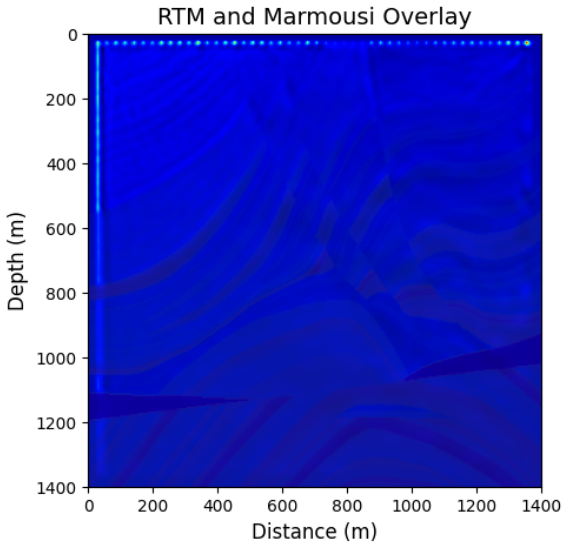

Figure 4: Structure comparison between RTM result and Marmousi model using 50 sources and a simulation time of 500 model seconds.

to produce the exact fidelity shown in the original Marmousi model, although this is note entirely unexpected. The difference is due in part to the spatial discretization limitations of the model in the computational calculation, as well as the interference of signals. The diminished resolution in the subsurface can also be handled by increasing the time the model is allowed to run, as is evident from the comparison between Figures 4 and 6.

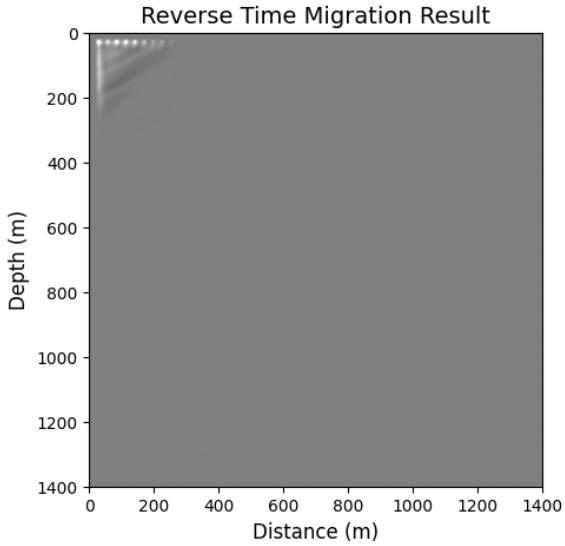

Figure 5: RTM result after running the simulation for 3,000 model seconds with 50 evenly distributed sources at 28m intervals.

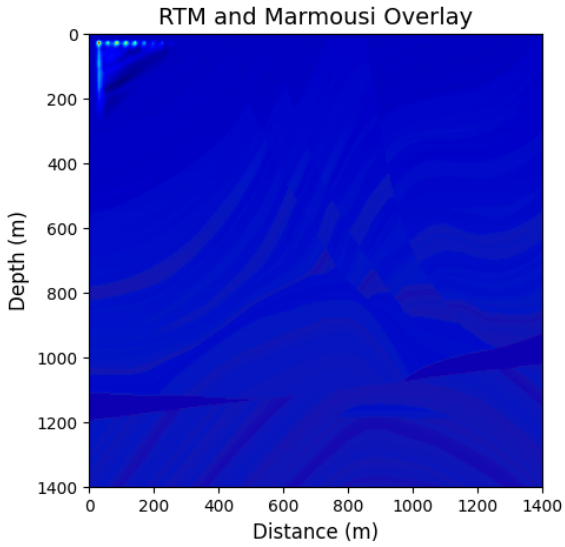

Figure 6: Structure comparison between RTM result and Marmousi model using 50 sources and a simulation time of 3,000 model seconds.

DISCUSSION

The first deployment of the model introduced a single source as depicted in Figure 7. However, as discussed previously, a multi-source arrangement can be calculated and summed to increase model resolution.

After testing a variety of different source locations, I found that when the sources were densely deployed, it became difficult to detect features in the near subsurface due to an extreme amount of scattering. Figure 8 displays the loss of resolution in the

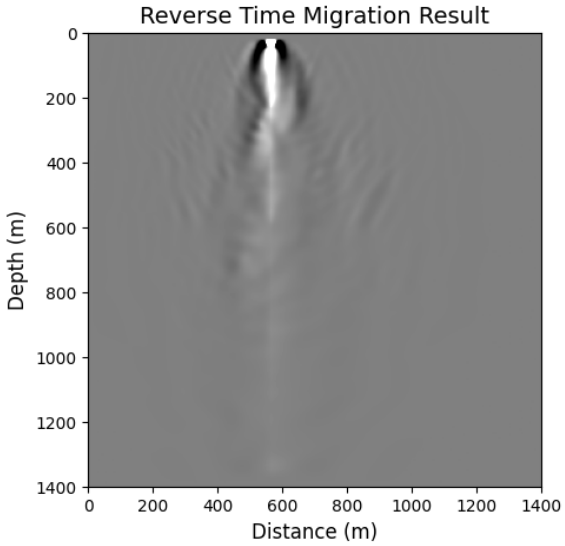

Figure 7: RTM result from a simulation of 1,500 model seconds with a single source point at [x=560m,y=28m].

near subsurface with densely deployed sources.

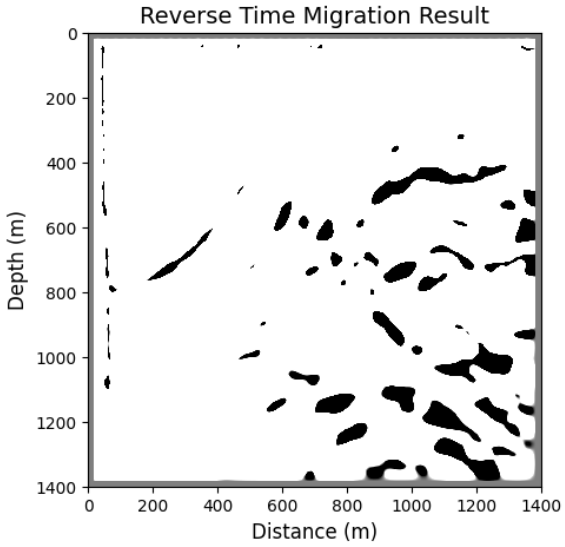

Figure 8: RTM result from simulation of 3,000 model seconds with 50 evenly distributed sources at 28 m intervals.

To combat this issue, the model output must be appropriately scaled for each scenario with a different numbers of receivers. For this reason, I chose a standard implementation with evenly distributed source locations with a width of 28 meters. I also tested a range of total run times to ensure that the wavelet was able to sufficiently propagate to the bottom boundary of the model. From the various simulation times tested, I believe that the minimum model time needed to sample features under 1000 meters is 1500 seconds. Figures 5 and 6 display the lack of penetration depth that occurs when the model is not run for a sufficiently long period, while Figures 9 and 10 are the RTM and overlay results from a simulation time of 1500 seconds.

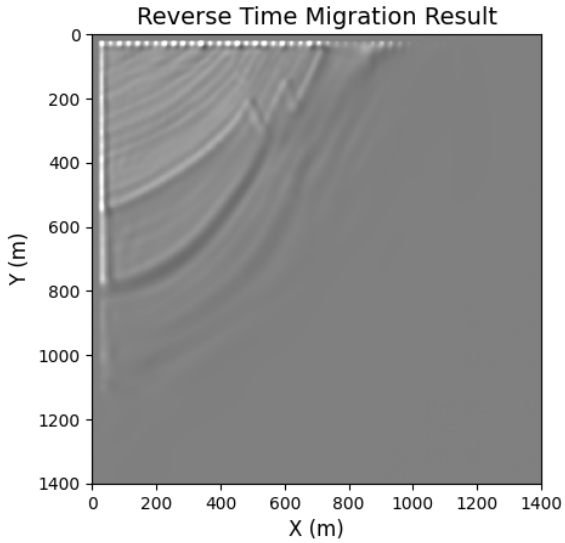

Figure 9: RTM result from simulation of 1,500 model seconds with 50 evenly distributed sources at 28 m intervals.

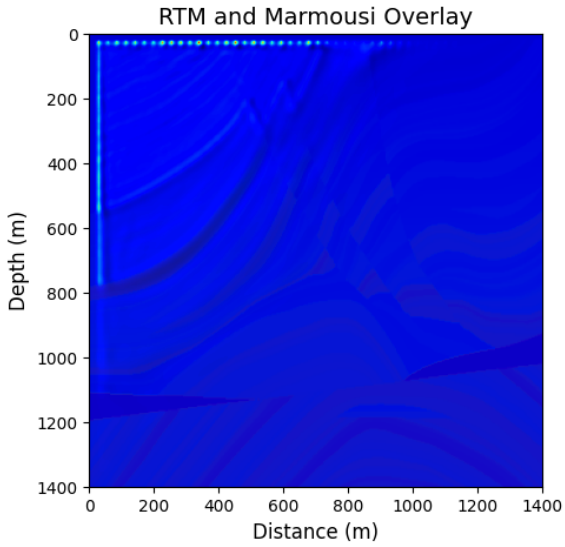

Figure 10: Structure comparison between RTM result and Marmousi model after a simulation of 1,500 model seconds.

Due to the increased attenuation from scattering as the wave travels through the model, the strength of the signal fades with depth. For this reason, the coloring scheme in the near surface of the RTM model appears to be much stronger. However, because the RTM method does not solve for the velocity in the medium, but rather the reflection points, the strength of the signal, and thus the color, does not relay any physical knowledge about the material at those locations. Appendix A includes the results from several other source setups and time simulations.

CONCLUSIONS

From the comparison between the Marmousi model and the calculated RTM result, it is clear that the RTM method is able to distinguish reflection boundaries in the subsurface. Although the RTM procedure does not perfectly match the the structure of the Marmousi model, they are in very close agreement. For models with a simpler velocity structure, the RTM method would produce even more accurate results since the extreme scattering in the Marmousi model's near surface would not impede wave propagation to greater depths. It is clear that longer simulation times are an incredibly important factor in increased model resolution, but it also comes at the expense of longer computation times.

For the standard implementation of the RTM process, the model best resolves images in the near subsurface. Structures in the deeper interior can clearly be seen when longer simulation times and denser source deployments are used, but the fidelity still pales in comparison to the results from the shallow reflections.

APPENDIX A

The images in this section are a variety of RTM results and their subsequent overlays against the Marmousi for a variety of simulation times not discussed in the paper.

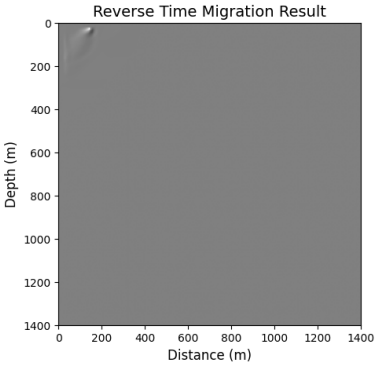

Figure A-1: RTM result from simulation of 500 model seconds with 10 evenly distributed sources at 140 m intervals.

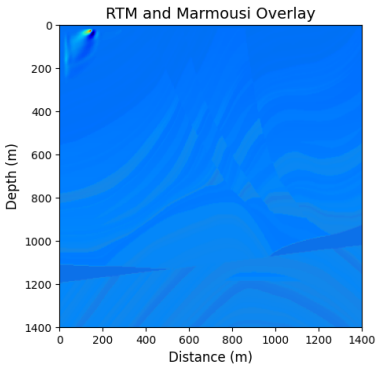

Figure A-2: Structure comparison between RTM result and Marmousi model using 10 sources and a simulation time of 500 model seconds.

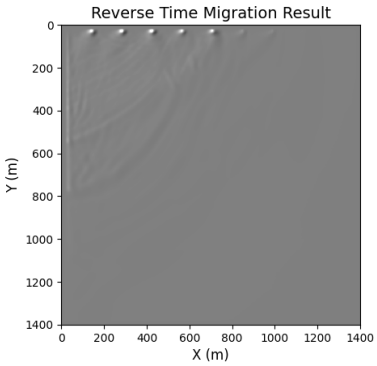

Figure A-3: RTM result from simulation of 1,500 model seconds with 10 evenly distributed sources at 140 m intervals.

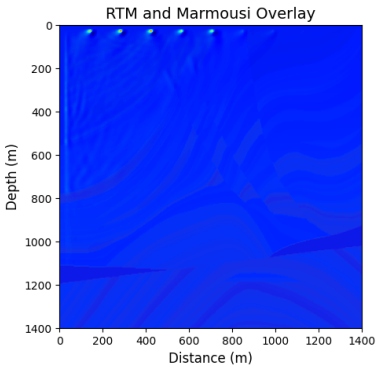

Figure A-4: Structure comparison between RTM result and Marmousi model using 10 sources and a simulation time of 1,500 model seconds.